

# Dynamic Programming-Based Offline Redundancy Resolution of Redundant Manipulators Along Prescribed Paths with Real-Time Adjustment

Zhihang Yin<sup>a,1</sup>, Fa Wu<sup>b,1</sup>, Ziqian Wang<sup>c</sup>, Jianmin Yang<sup>d</sup>, Jiyong Tan<sup>e,\*</sup> and Dexing Kong<sup>a,\*</sup>

<sup>a</sup>School of Mathematical Sciences, Zhejiang University, Xihu, Hangzhou, 310058, Zhejiang, China

<sup>b</sup>Zhejiang Demetics Medical Technology Co., Ltd., Xihu, Hangzhou, 310012, Zhejiang, China

<sup>c</sup>Department of Human Development, Teachers College, Columbia University, New York, 10027, NY, United States

<sup>d</sup>Zhejiang College of Sports, Hangzhou, 311231, Zhejiang, China

<sup>e</sup>Shenzhen Institute for Advanced Study, University of Electronic Science and Technology of China, Shenzhen, 610056, Guangdong, China

## ARTICLE INFO

### Keywords:

Robot programming  
manipulator motion planning  
optimal control  
optimization methods

## ABSTRACT

Traditional offline redundancy resolution of trajectories for redundant manipulators involves computing inverse kinematic solutions for Cartesian space paths, constraining the manipulator to a fixed path without real-time adjustments. Online redundancy resolution can achieve real-time adjustment of paths, but it cannot consider subsequent path points, leading to the possibility of the manipulator being forced to stop mid-motion due to joint constraints. To address this, this paper introduces a dynamic programming-based offline redundancy resolution for redundant manipulators along prescribed paths with real-time adjustment. The proposed method allows the manipulator to move along a prescribed path while implementing real-time adjustment along the normal to the path. Using Dynamic Programming, the proposed approach computes a global maximum for the variation of adjustment coefficients. As long as the coefficient variation between adjacent sampling path points does not exceed this limit, the algorithm provides the next path point's joint angles based on the current joint angles, enabling the end-effector to achieve the adjusted Cartesian pose. The main innovation of this paper lies in augmenting traditional offline optimal planning with real-time adjustment capabilities, achieving a fusion of offline planning and online planning.

## 1. Introduction

In many applications of robotics, such as ultrasound scanning robots(Li, Xu and Meng, 2021), massage robots(Ma, Yao, Ni and Zhu, 2005), polishing robots(Zeng, Zhu, Gao, Ji, Ansari and Lu, 2023; Xenya and Cortesao, 2023), and others, it is necessary for the robot to move precisely along a pre-planned path in a three-dimensional workspace. When performing these tasks, non-redundant manipulators are easily limited by singular points and joint ranges, making it difficult for them to reach certain specific poses along the given path (Fahimi, 2009;2008:), so redundant manipulators are preferred.

In this paper, we consider the application scenario of robotic ultrasound scanning using a 7-degree-of-freedom redundant manipulator. Equipped with an ultrasound probe at its end effector, the manipulator acquires ultrasound images in close proximity to the patient's skin. Consequently, the manipulator needs to move along a Cartesian space path specified according to the patient's body surface, aiming to complete the scan as seamlessly as possible to enhance the quality and efficiency of the diagnose.

When the scanning probe makes contact with the skin, it causes a certain deformation. Additionally, the patient's breathing and other movements lead to deviations between

the actual human body and the 3D model previously established. Therefore, we aim for the manipulator to adjust the path along the normal direction during the scanning process. This adjustment ensures better conformity of the probe to the patient's body surface, thereby enhancing scanning efficiency while maintaining patient safety and comfort.

Due to the redundancy of the manipulator we use, a given end-effector pose can correspond to an infinite number of possible joint configurations, known as its inverse kinematic solutions. Although these joint configurations can all position the end-effector at the same pose, the range of joint configurations achievable during subsequent motion will differ due to constraints on joint angles, velocities, and other factors, leading to variations in the range of poses that can be later reached. Therefore, selecting the optimal solution from the infinite possible inverse kinematic solutions is crucial for the completeness of subsequent motion. This pertains to the redundancy resolution problem in redundant manipulators. The redundancy resolution algorithms for manipulators can be broadly categorized into two types: online planning and offline planning.

In online planning, the inverse kinematic solution of the target pose are computed based on the current joint parameters of the manipulator. This method only considers local path points, disregarding the restrictions of the current joint positions on subsequent motion, and thus cannot guarantee complete motion along a given path. The Cartesian pose controller integrated within the manipulator that we utilize belongs to this category. We will demonstrate its

\*Corresponding author

✉ scutjy2015@163.com (J. Tan); dxkong@zju.edu.cn (D. Kong)

ORCID(S): 0000-0001-6356-1743 (J. Tan); 0000-0001-9339-8086 (D.

Kong)

<sup>1</sup>The two authors contribute equally to this work.

disadvantage through experiments in Section IV. On the other hand, online planning algorithms inherently consider only the current state of the manipulator and the target pose, allowing for easy path adjustments. Widely used impedance control (Hogan, 1984; Song, Yu and Zhang, 2017; He, Dong and Sun, 2016; Ficuciello, Villani and Siciliano, 2015) falls into this category of algorithms.

To prevent the manipulator from halting its motion due to joint limitations during operation, a viable approach is to employ an offline planning algorithm. Such algorithms consider all the path points along the manipulator's path simultaneously before its motion, thoroughly addressing the restrictions imposed by the joint angles on subsequent motion. By considering all path points, the obtained inverse kinematic solutions can satisfy various joint constraints, such as those related to angle and velocity. However, due to the nonlinearity of the inverse kinematic mapping of the manipulator, changing the pose of a single path point and calculating its corresponding joint angles does not allow for a simple linear calculation of the subsequent points' corresponding joint angles. Instead, the inverse kinematic solutions of all subsequent Cartesian poses need to be re-computed using the complex algorithm. This process requires a significant amount of time, making real-time path adjustments challenging.

We aspire for the manipulator to traverse a path without interruptions while also being capable of real-time path adjustments during its motion. Therefore, we aim to enhance the offline planning algorithm to integrate real-time adjustment functionalities. Driven by this concept, we propose a dynamic programming-based offline optimal planning algorithm of redundant manipulators along prescribed paths with real-time adjustment. With this algorithm, the manipulator can complete its motion along the path while allowing real-time adjustments to the path.

### 1.1. Related Work

The key to our study lies in solving the redundancy resolution of a redundant manipulator. Redundancy resolution can be done in the velocity or position level (Fahimi, 2009; 2008;). Algorithms designed on the joint velocity level involve online computing the pseudoinverse of the Jacobian matrix associated with the forward kinematics of the controlled manipulator (Zhang, Li and Zhou, 2019). Such algorithm is online, as the manipulator moves, it calculates the joint angles for the next time step based on the current joint parameters and the expected Cartesian pose for the next time step. In (Zhong, Zhang, Zhai, Li, Xu, Pan and Zhou, 2023), a real-time optimization problem is established by considering the joint constraints of the manipulator as constraints, with the error between the current trajectory of the manipulator and the expected trajectory as the optimization objective. RNN is used for real-time optimization.

However, as mentioned before, such velocity-based algorithm overlooks the influence of the current manipulator joint angles on the subsequent motion of the robot. As the manipulator moves, the joint angles of some joints may reach

limits, causing the manipulator to jam and preventing further motion. The algorithm proposed in (Xu and Sun, 2018) keeps the manipulator closer to the mid-joint position of the joint limits to eliminate the danger of joint limits. However, due to the uncertainty of subsequent paths, this still does not guarantee that the joint angles of the manipulator will not reach their limits. Simultaneously, there are certain poses where a specific joint angle must approach a critical value. Therefore, to ensure that the manipulator does not jam during its operation, it is necessary to consider all points along the entire path and seek a global optimal solution.

Algorithms designed on the joint position level generally introduce appropriate parameters to obtain the inverse kinematic solutions at various points along the path. Subsequently, by designing a global energy function, an optimization problem is formulated to determine the parameter values at each point, thereby achieving the global optimal solution for redundancy resolution along the path. Due to the simultaneous consideration of all path points and the computation of all inverse kinematic solutions, this type of algorithm belongs to offline planning and needs to be completed before the manipulator's motion. A joint parametrization method for redundancy resolution is proposed by (Lee and Bejczy, 1991). In their method, redundant joints are selected appropriately and the joint displacements themselves are regarded as the redundancy parameters, obtaining a closed-form of inverse kinematic solution. Other parameterization methods, such as those proposed in (Shimizu, Kakuya, Yoon, Kitagaki and Kosuge, 2008), can also be selected based on the specific structure of the manipulator.

Through parameterization, determining the inverse kinematic solution for the manipulator's path transforms into finding the parameter values for each path point. This converts the problem into an optimization problem, where the objective of the optimization is determined by the practical requirements of the task. The algorithm proposed in (Schappler, 2023; Ferrentino, Savino, Franchi and Chiacchio, 2023) use dynamic programming for optimal planning of redundant robots along prescribed paths. Based on the specific requirements of different practical tasks, an arbitrary energy function can be established as the objective of the optimization problem. Constraints can also be converted into constraints for the optimization problem through mathematical modeling.

Dynamic programming is a mathematical method for solving a class of optimization problems. It breaks down complex problems into a series of interconnected and overlapping subproblems, and combines the solutions of these subproblems recursively to obtain the optimal solution to the original problem (Simpson, 1961; Zietz, 2007). Using the dynamic programming algorithm, we can determine the globally optimal solution for redundancy resolution corresponding to the prescribed path, ensuring that the joint angle motion at every moment complies with the manipulator's constraints, thereby preventing the manipulator from malfunctioning and stopping during operation.

To ensure the integrity of the manipulator's motion, this paper opts to use the dynamic programming-based offline planning algorithm as the foundation, combined with a real-time control algorithm to address the problem proposed in this study.

## 1.2. Paper Contribution and Organization

The main contribution of this paper is the introduction of real-time adjustment functionality to the traditional offline optimal planning algorithm for redundant manipulators along prescribed paths. This enables the manipulator to adapt the path in real time according to the environmental conditions. This paper presents three main innovations:

- Augmenting traditional offline optimal planning with real-time adjustment capabilities achieves a fusion of offline and online planning and enables the manipulator to adapt instantly to changes in the working environment and execute pre-defined tasks more effectively.
- For the same pose, different inverse kinematic solutions are chosen based on the current joint angles, ensuring that the motion of each joint complies with the constraints.
- The design of the dynamic programming algorithm enables the simultaneous determination of the inverse kinematic solution for the path and the maximum variation in path adjustment parameters.

This paper is organized as follows. First, the mathematical model of the problem is described in section II. Then, the dynamic programming-based offline optimal planning algorithm of redundant manipulators along prescribed paths with real-time adjustment is proposed in section III. Finally, we tested the algorithm using test paths and randomly generated adjustment parameters, thereby demonstrating the reliability of the algorithm in section IV.

## 2. Preliminaries and problem formulation

In our work, we will take the Franka 7-DOF manipulator (Haddadin, Parusel, Johannsmeier, Golz, Gabl, Walch, Sabaghian, Jaehne, Hausperger and Haddadin, 2022) for study and experimentation. The host system communicates with the manipulator at a frequency of 1000Hz. The host system is capable of real-time access to various motion parameters of the manipulator, enabling it to send control commands for the motion of the manipulator. Therefore, we choose to discretize the pre-planned path in Cartesian space, ensuring that the sampling interval between adjacent path points is a multiple of the communication period of the manipulator.

For a given path, we refer to the points that specify the corresponding Cartesian poses as sampling points, and the points at which the manipulator needs to communicate with the host and receive control signals as communication points. A sampling point necessarily corresponds to a communication point, while a communication point may not be a sampling point. The host system, based on real-time information obtained from sensor readings, adjusts the positions of subsequent path points along the normal to the path at sampling points.

Given a discrete path  $\{\mathbf{T}_{EEi}\}$  with  $n+1$  sampling points in Cartesian space,  $i$  represents the index of sampling points ranging from 0 to  $n$  and  $\mathbf{T}_{EEi}$  denotes the end effector pose of the  $i$ -th sampling point.  $\mathbf{T}_{EEi}$  is a homogeneous transformation matrix, which can be represented by a three-dimensional rotation matrix and a three-dimensional translation vector:

$$\mathbf{T}_{EEi} = \begin{bmatrix} \mathbf{R}_{EEi} & \mathbf{p}_{EEi} \\ \mathbf{0}_{1 \times 3} & 1 \end{bmatrix} \quad (1)$$

where  $\mathbf{R}_{EEi}$  is the rotation matrix of the end effector of the  $i$ th sampling point, and  $\mathbf{p}_{EEi}$  is the translation vector. The host will calculate the bounded adjustment coefficients  $y_i$  in real time and adjust the end effector pose of the  $i$ th sampling point to  $\hat{\mathbf{T}}_{EEi}(y_i)$  according to the normal vector  $\mathbf{Z}_i$  to the path:

$$\hat{\mathbf{T}}_{EEi}(y_i) = \begin{bmatrix} \mathbf{R}_{EEi} & \mathbf{p}_{EEi} + y_i \mathbf{Z}_i \\ \mathbf{0}_{1 \times 3} & 1 \end{bmatrix} \quad (2)$$

We will only consider the limitations on joint angle and velocity at first. Constraints on acceleration and jerk can be achieved through velocity limitations and further algorithmic adjustments. The angular velocity of the manipulator's joints is limited by  $\mathbf{q}_{\max}$ , and the joint angles have both lower and upper bounds, denoted as  $\mathbf{q}_{\min}$  and  $\mathbf{q}_{\max}$  respectively.

Due to limitations in the angular velocity of the manipulator's joints, the manipulator may fail to reach the adjusted position when the adjustment values undergo significant changes. Therefore, we have to determine a method for computing the inverse kinematic solution and setting an upper bound on the change in the adjustment value  $y_i$ . The upper bound  $\delta$  should be as large as possible to enable the manipulator to adjust the path to the maximum extent.

In offline planning, the assurance that the manipulator's trajectory complies with the joint constraints is established by predetermining the joint angles of each path point before the motion, ensuring that these angles satisfy the constraints. Building upon this concept, we want to calculate the joint angles corresponding to all path points in advance, which is quite challenging for the infinite possibilities of an adjusted path. Therefore, we divide the range of  $y_i$  into  $2o$  equal parts and discretize the coefficients to  $2o+1$  discrete values  $\{b_{-o}, b_{-o+1}, \dots, b_o\}$  to maintain a finite set of potential path scenarios. Denote  $y_i$  as  $b_{c_i}$ , and the restriction  $\delta$  on the variation of  $y_i$  implies a restriction on the variation of  $c_i$ , denoted as  $d$ . In other words, depending on the different values of  $y_i, y_{i+1}$  can have at most  $2d+1$  different values.

Taking into account the constraints imposed by the joint angles of the previous sampling point on the current sampling point, for different adjusted paths, despite the manipulator having the same Cartesian pose at the current sampling point, the pose and joint angles of the previous sampling point may differ, leading to different constraints on the joint angles at the current sampling point. Thus, even with identical Cartesian poses, the corresponding joint angles differ. We will compute the inverse kinematic solution for the target pose based on the joint angles of the previous

sampling point, in other words, obtaining the inverse kinematic mapping  $\mathbf{q}_i = f^{-1}(\hat{\mathbf{T}}_{EEi}(y_i), \mathbf{q}_{i-1})$ .

Deriving the inverse kinematic solutions based on the current joint angles of the manipulator resembles online planning. The distinction lies in the fact that we do not compute the inverse kinematic solutions in real-time, but rather perform all calculations before the manipulator's motion commences, ensuring uninterrupted motion of the manipulator under all feasible adjustment paths.

The problem we aim to address is as follows: to find the theoretical global maximum value for  $d$ , along with an inverse kinematic mapping  $f^{-1}$ , such that: for any  $\{c_n\}$  that satisfies:

$$\begin{aligned} c_0 &= 0 \\ |c_i - c_{i-1}| &\leq d, \forall i \in \{1, 2, \dots, n\} \end{aligned} \quad (3)$$

$\mathbf{q}_i = f^{-1}(\hat{\mathbf{T}}_{EEi}(b_{c_i}), \mathbf{q}_{i-1})$  is an inverse kinematic solution of  $\hat{\mathbf{T}}_{EEi}(b_{c_i})$ , and  $\mathbf{q}_i$  satisfies the following equation:

$$\begin{aligned} q_{\min,c} &\leq q_{i,c} \leq q_{\max,c}, i = 0, 1, \dots, n; c = 1, 2, \dots, 7 \\ |\dot{q}_{i,c}| &\leq \dot{q}_{\max,c}, i = 1, 2, \dots, n; c = 1, 2, \dots, 7 \end{aligned} \quad (4)$$

where  $q_{\min,c}, q_{\max,c}, q_{i,c}, \dot{q}_{i,c}, \dot{q}_{\max,c}$  represent the  $c$ -th components of vectors  $\mathbf{q}_{\min}, \mathbf{q}_{\max}, \mathbf{q}_i, \dot{\mathbf{q}}_i, \dot{\mathbf{q}}_{\max}$  respectively. The angular velocities of joints can be easily calculated by definition:

$$\dot{\mathbf{q}}_i = \frac{\mathbf{q}_i - \mathbf{q}_{i-1}}{t_0}, i = 1, 2, \dots, n \quad (5)$$

The process of the proposed algorithm is roughly illustrated as in Figure 1. The algorithm is roughly divided into two parts: the offline planning before the manipulator's motion and the real-time interaction with the manipulator during its motion, including the real-time adjustment of the path and motion compensation between adjacent sampling points.

### 3. Algorithms

In this section, we will use dynamic programming to obtain the maximum  $d$  and the inverse kinematic mapping  $f^{-1}$ . Subsequently, we will employ motion compensation algorithm to ensure that the joint trajectory satisfies constraints on acceleration and jerk, enabling it to operate on the actual hardware.

#### 3.1. Inverse Kinematics

Before seeking the redundancy resolution for the entire path, it is worthwhile to first consider the inverse kinematic solution corresponding to a single Cartesian pose  $\mathbf{T}_{EE}$ . Due to the redundancy of the 7-DOF manipulator, there exist infinitely many inverse kinematic solutions.

Take the Franka Emika manipulator we use for experimental purposes in this study as an example. It is a nimble lightweight robot with 7 degrees of freedom and highly

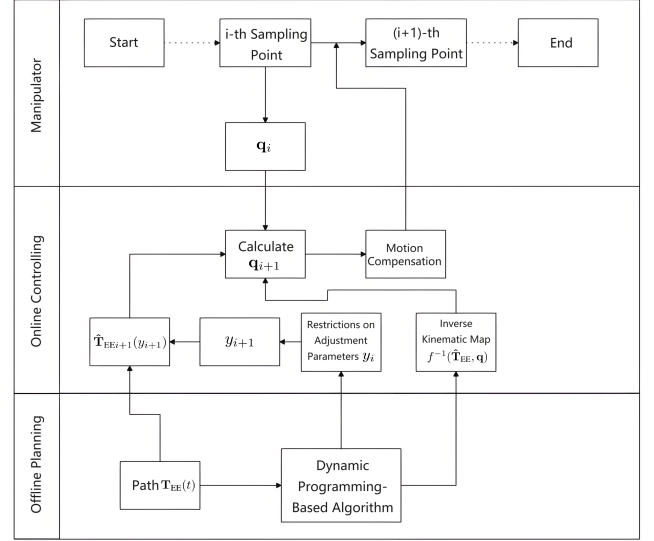
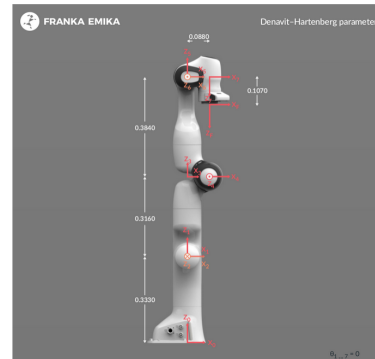


**Figure 1:** The process of the proposed algorithm. The algorithm is roughly divided into two parts: the offline planning before the manipulator's motion and the real-time interaction with the manipulator during its motion, including the real-time adjustment of the path and motion compensation between adjacent sampling points.

sensitive sensors. Figure 2 shows the Denavit-Hartenberg parameters of the Franka Emika manipulator, and Table 1 shows the limits of the joints of the manipulator<sup>2</sup>.



$i$	$a_i$	$\alpha_i$	$d_i$	$\theta_i$
1	0	0	$d_1$	$q_1$
2	0	$-\pi/2$	0	$q_2$
3	0	$\pi/2$	$d_3$	$q_3$
4	$a_4$	$\pi/2$	0	$q_4$
5	$a_5$	$-\pi/2$	$d_5$	$q_5$
6	0	$\pi/2$	0	$q_6$
7	$a_7$	$\pi/2$	0	$q_7$
8	0	0	$d_f$	0

**Figure 2:** Denavit-Hartenberg frames and table of parameters for the Franka Emika robot. In this figure, joint angles  $q_{1,\dots,7} = 0$ . The reference frames follow the modified Denavit-Hartenberg convention,  $d_1 = 0.333\text{m}$ ,  $d_3 = 0.316\text{m}$ ,  $d_5 = 0.384\text{m}$ ,  $d_f = 0.107\text{m}$ ,  $a_4 = 0.0825\text{m}$ ,  $a_5 = -0.0825\text{m}$ ,  $a_7 = 0.088\text{m}$ .

By employing the parameterization technique (Ferrentino and Chiacchio) and geometrical analysis (Tittel, 2021), we can derive closed-form inverse kinematics solutions for the manipulator. Following (Lee and Bejczy, 1991), a certain joint angle can be fixed as a parameter. The algorithm proposed in (He and Liu, 2021) calculates the inverse kinematic solutions of the Franka robot by taking  $q_7$ , the joint angle of

<sup>2</sup><https://frankaemika.github.io/docs/>

**Table 1**  
Limits of Joints

Name	Joint 1	Joint 2	Joint 3	Joint 4	Joint 5	Joint 6	Joint 7	Unit
$\mathbf{q}_{\max}$	2.8973	1.7628	2.8973	-0.0698	2.8973	3.7525	2.8973	rad
$\mathbf{q}_{\min}$	-2.8973	-1.7628	-2.8973	-3.0718	-2.8973	-0.0175	-2.8973	rad
$\dot{\mathbf{q}}_{\max}$	2.1750	2.1750	2.1750	2.1750	2.6100	2.6100	2.6100	$\frac{\text{rad}}{\text{s}}$
$\ddot{\mathbf{q}}_{\max}$	15	7.5	10	12.5	15	20	20	$\frac{\text{rad}}{\text{s}^2}$
$\dddot{\mathbf{q}}_{\max}$	7500	3750	5000	6250	7500	10000	10000	$\frac{\text{rad}}{\text{s}^3}$

the 7th joint of the manipulator, as a parameter. Once  $q_7$  is specified, the manipulator can be considered as a 6-degree-of-freedom one. When a solution exists, there are three possible scenarios that lead to multiple solutions, resulting in up to 8 sets of solutions. These multiple solutions can be mutually converted when they exist. By considering the constraints on each joint angle, an analysis is conducted to exclude the multiple solutions while preserving the existence of the solutions through the imposition of restrictions on the joint angles. From this, we can obtain a bijective inverse kinematic mapping  $f_{q_7}^{-1}$  within the workspace of the 6-DOF manipulator:

$$[q_1, q_2, \dots, q_6]^T = f_{q_7}^{-1}(\mathbf{T}_{EE}) \quad (6)$$

Thus, we have obtained the parameterized inverse kinematic solution for the 7-DOF manipulator:

$$\begin{aligned} \mathbf{q} &= \tilde{f}^{-1}(\mathbf{T}_{EE}, q_7) \\ &= \begin{bmatrix} f_{q_7}^{-1}(\mathbf{T}_{EE}) \\ q_7 \end{bmatrix} \end{aligned} \quad (7)$$

During the computation of the inverse kinematic solutions, we also incorporate avoidance strategies for singularity. In robotics, the relationship between joint velocities and Cartesian velocities at the end-effector of a manipulator is commonly expressed using the Jacobian matrix as follows:

$$\mathbf{v} = \mathbf{J}(\mathbf{q})\dot{\mathbf{q}} \quad (8)$$

where  $\mathbf{v}$  represents the Cartesian velocity vector and  $\mathbf{J}$  denotes the Jacobian matrix. When the Jacobian matrix becomes singular, the manipulator loses one or more degrees of freedom, resulting in restricted motion in a particular direction in Cartesian space regardless of the chosen joint velocities. This limitation is known as singularity in the robot's motion (Fahimi, 2009; 2008;).

After obtaining a set of joint angles, we can compute the corresponding Jacobian matrix, thereby excluding singular configurations of the manipulator. Additionally, before computing the inverse kinematic solutions, we can derive the expression of the Jacobian matrix with respect to the joint angles and determine the conditions that the joint angles must satisfy for the matrix to be singular. This approach enables the avoidance of singularity with reduced computational overhead.

In this paper, we will adopt another discretization approach: dividing the range of  $q_7$  into  $m - 1$  equal parts, thereby restricting the values of  $q_7$  to  $m$  discrete values  $\{a_1, a_2, \dots, a_m\}$ . As  $m$  increases, we consider a larger number of possibilities, leading to improved algorithm performance. When  $m$  is small, it still presents a viable path for the normal operation of the manipulator, due to its compliance with all the constraints imposed on the joints.

For other redundant manipulators with potentially greater degrees of freedom, the method for solving the inverse kinematics remains the same, albeit requiring the introduction of additional parameters.

### 3.2. Dynamic Programming-Based Algorithm

It should be noted that given the end-effector pose  $\mathbf{T}_{EE}$ , not every  $q_7$  value can yield a corresponding inverse kinematic solution due to various restrictions on the manipulator joint angles and mechanical structure. The following test path serves as an example:

$$\mathbf{T}_{EE}(t) = \begin{bmatrix} \cos(\theta(t)) & \sin(\theta(t)) & 0 & 0.6 + 0.1 \cos(\theta(t)) \\ \sin(\theta(t)) & -\cos(\theta(t)) & 0 & 0.1 \sin(\theta(t)) \\ 0 & 0 & -1 & 0.1 \\ 0 & 0 & 0 & 1 \end{bmatrix} \quad (9)$$

where  $\theta(t) = \frac{2\pi}{t_{\max}}t - \pi, 0 \leq t \leq t_{\max}$  and the duration  $t_{\max}$  is 10 seconds.

The existence of solutions corresponding to each  $\mathbf{T}_{EE}(t)$  and  $q_7$  is depicted in a figure, where the black regions indicate the existence of the inverse kinematic solutions, as shown in Figure 3.

For the inverse kinematic solution of a fixed path, it is tantamount to finding a continuous curve within the blue region in Figure 3 that connects  $t = 0$  and  $t = 10$ , while ensuring that adjacent points on the curve satisfy the manipulator's constraints on joint velocities. Other joint angles, such as the point in the lower left blue section in Figure 3, although representing an inverse kinematic solution for the path point, are not contiguous with the subsequent blue sections, thus causing a discontinuity in motion. This underscores the necessity of anticipating subsequent path points in advance.

The problem under investigation in this study introduces an adjustment parameter,  $y$ . We can depict the existence of

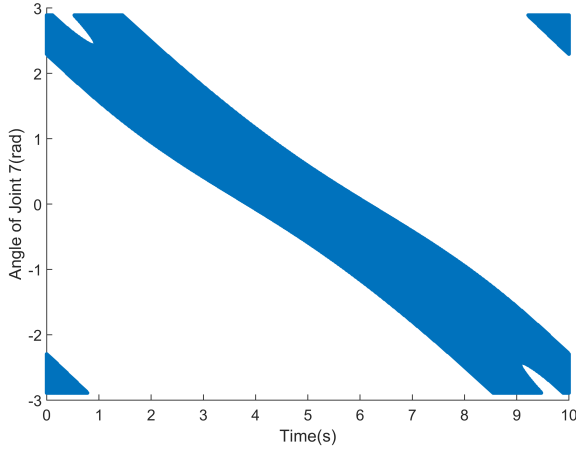


**Figure 3:** The existence of solutions corresponding to each  $\hat{\mathbf{T}}_{EE}(t)$  and  $q_7$  is depicted in a figure, where the black regions indicate the existence of the inverse kinematic solutions.

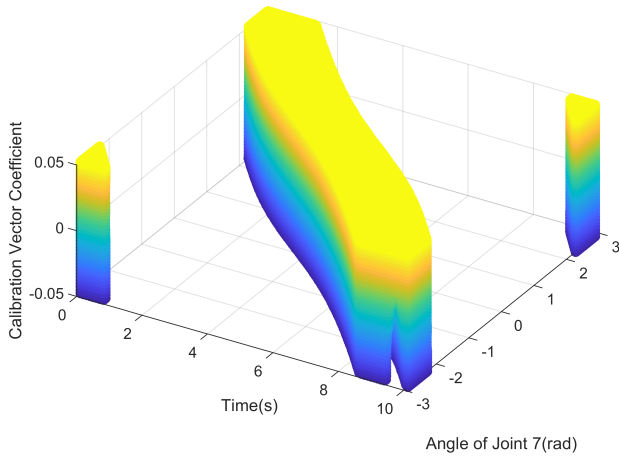


**Figure 4:** The existence of solutions corresponding to each  $\hat{\mathbf{T}}_{EE}(t)$ ,  $y$  and  $q_7$  is depicted in a figure, where the colored regions indicate the existence of the inverse kinematic solutions.

the inverse kinematic solution for  $\mathbf{T}_{EE}$  corresponding to  $q_7$  and  $y$  in a three-dimensional coordinate system. The colored region in the graph indicates the existence of the corresponding solutions, as illustrated in Figure 4.

Similar to the fixed path problem, we need to solve the inverse kinematics within the colored region of the three-dimensional coordinate system in Figure 4. Denote  $\tilde{f}^{-1}(\hat{\mathbf{T}}_{EEi}(b_k), a_j)$  as  $\bar{\mathbf{q}}_{i,j,k}$ . The colored point with Cartesian coordinates  $(i, j, k)$  in Figure 4 represents  $\bar{\mathbf{q}}_{i,j,k}$ . We aim to find the global maximum variation  $d$  between  $c_i$  and  $c_{i+1}$  for all  $i$ . To obtain this global maximum, we will employ a dynamic programming algorithm and construct a local energy function for each set of potential joint angles.

For the joint angles  $\bar{\mathbf{q}}_{i,j,k} = f^{-1}(\hat{\mathbf{T}}_{EEi}(b_k), a_j)$  of the manipulator, we can consider this path point as a new starting point and move along the original path to the endpoint with adjustment, thus forming a sub-path. On this sub-path,

we can define an energy function  $L(i, j, k)$  analogous to  $d$ :  $L(i, j, k)$  is the maximum  $d_i$ , such that for any  $\{y_n\}$  that satisfies:

$$\begin{aligned} c_i &= k, \mathbf{q}_i = \bar{\mathbf{q}}_{i,j,k} \\ |c_x - c_{x-1}| &\leq d_i, \forall x \in \{i+1, i+2, \dots, n\} \end{aligned} \quad (10)$$

$\mathbf{q}_x = f^{-1}(\hat{\mathbf{T}}_{EEi}(b_{c_x}), \mathbf{q}_{x-1})$  is an inverse kinematic solution of  $\hat{\mathbf{T}}_{EEi}(b_{c_x})$ , and  $\mathbf{q}_x$  satisfies the following equation:

$$\begin{aligned} q_{\min,c} &\leq q_{x,c} \leq q_{\max,c}, x = i, i+1, \dots, n; c = 1, 2, \dots, 7 \\ |\dot{q}_{x,c}| &\leq \dot{q}_{\max,c}, x = i+1, i+2, \dots, n; c = 1, 2, \dots, 7 \end{aligned} \quad (11)$$

It's obvious that :

$$\max d = \max_{j=1}^m L(0, j, 0) \quad (12)$$

The potential pose of the next sampling point is  $\hat{\mathbf{T}}_{EEi+1}(b_{k+e})$ , where  $|e| \leq L(i, j, k)$ , and  $|k+e| \leq o$ . Hence, for all  $\bar{\mathbf{q}}_{i,j,k}$ , we will recursively calculate  $L(i, j, k)$  and define all inverse mappings  $f^{-1}(\hat{\mathbf{T}}_{EEi+1}(b_{k+e}), \bar{\mathbf{q}}_{i,j,k})$ . Assuming  $\bar{\mathbf{q}}_{i,j,k}$  represents a set of feasible joint angles achievable by the manipulator in the final path, the path originating from it is necessarily a sub-path of the original trajectory. By definition, we can deduce that  $d \leq L(i, j, k)$ . Therefore, the inverse mappings we compute can encompass all inverse mappings involved in the final path.

For any chosen set of  $i, j$ , and  $k$ , and for any non-negative integer  $s$ , if  $L(i, j, k) \geq s$ , according to the definition, for any  $\{c_n\}$  satisfying  $|c_x - c_{x-1}| \leq s$  for all  $x = i+1, i+2, \dots, n$  and  $c_i = k$ , we have  $\mathbf{q}_i = \bar{\mathbf{q}}_{i,j,k}$ ,  $\mathbf{q}_x = f^{-1}(\hat{\mathbf{T}}_{EEi}(b_{c_x}), \mathbf{q}_{x-1})$  as an inverse kinematic solution of  $\hat{\mathbf{T}}_{EEi}(b_{c_x})$ , and  $\mathbf{q}_x$  satisfies the constraints. Take  $c_{i+1} = k+e$  which satisfies  $|e| \leq s$  and  $|k+e| \leq o$ .  $|c_{i+1} - c_i| \leq s$ , thus there exists a  $j_e$  such that  $\bar{\mathbf{q}}_{i+1,j_e,k+e} = f^{-1}(\hat{\mathbf{T}}_{EEi+1}(b_{k+e}), \mathbf{q}_i)$ .  $\bar{\mathbf{q}}_{i+1,j_e,k+e}$  is a pathpoint of the sub-path starting from  $\bar{\mathbf{q}}_{i,j,k}$ , thus for any  $\{c_n\}$  satisfying  $|c_x - c_{x-1}| \leq s$  for all  $x = i+2, i+3, \dots, n$  and  $c_{i+1} = k+e$ , we can take  $c_i = k$  and use the  $\mathbf{q}_x$  calculated from the sub-path starting from  $\bar{\mathbf{q}}_{i,j,k}$  as the inverse kinematic solution of  $\hat{\mathbf{T}}_{EEi}(b_{c_x})$  in the sub-path starting from  $\bar{\mathbf{q}}_{i+1,j_e,k+e}$ . It inherently satisfies the constraints. From definition, we have  $L(i+1, j_e, k+e) \geq s$ . Thus, if  $L(i, j, k) \geq s$ , for any  $e$  satisfying  $|e| \leq s$  and  $|k+e| \leq o$ , there exists a  $j_e$  such that  $L(i+1, j_e, k+e) \geq s$ .

Conversely, if for any  $e$  satisfying  $|e| \leq s$  and  $|k+e| \leq o$ , there exists a  $j_e$  such that  $L(i+1, j_e, k+e) \geq s$  and  $\bar{\mathbf{q}}_{i+1,j_e,k+e}$  satisfies the constraints with  $\bar{\mathbf{q}}_{i,j,k}$ , then  $L(i, j, k) \geq s$ . For any  $\{c_n\}$  satisfying  $|c_x - c_{x-1}| \leq L(i, j, k)$  for all  $x = i+1, i+2, \dots, n$  and  $c_i = k$ , there's a certain  $e$  such that  $c_{i+1} = k+e$ . We can then use the  $\mathbf{q}_x$  calculated from the sub-path starting from  $\bar{\mathbf{q}}_{i+1,j_e,k+e}$  as the inverse kinematic solution of  $\hat{\mathbf{T}}_{EEi}(b_{c_x})$  in the sub-path starting from  $\bar{\mathbf{q}}_{i,j,k}$ . It inherently satisfies the constraints. From definition, we have

$L(i, j, k) \geq s$ . Thus, we have obtained the recursive property of  $L(i, j, k)$ .

For a fixed set of  $i, j$  and  $k$ , we will use the recursive property to calculate  $L(i, j, k)$  and define  $f^{-1}(\hat{\mathbf{T}}_{EEi+1}(b_{k+e}), \bar{\mathbf{q}}_{i,j,k})$  for any  $e$  satisfying  $|e| \leq L(i, j, k)$  and  $|k + e| \leq o$ . The inverse kinematic solution  $\bar{\mathbf{q}}_{i+1,j',k+e}$  of  $\hat{\mathbf{T}}_{EEi+1}(b_{k+e})$  that complies with the constraints and has the maximum  $L(i + 1, j', k + e)$  is denoted as  $\bar{\mathbf{q}}_{i+1,j_e,k+e}$ . We define:

$$f^{-1}(\hat{\mathbf{T}}_{EEi+1}(b_{k+e}), \bar{\mathbf{q}}_{i,j,k}) = \bar{\mathbf{q}}_{i+1,j_e,k+e} \quad (13)$$

We will start from  $i = n - 1$  and recursively calculate all the values of  $L(i, j, k)$  with  $i$  moving backward. For  $\bar{\mathbf{q}}_{n-1,j,k}$ , we simply need to ensure that the joint angles at the next sampling point satisfies the constraints. We start with  $d_{n-1}$  at 0 and increase it by 1 each time, checking if the compliant solutions  $\bar{\mathbf{q}}_{i+1,j-d_{n-1},k-d_{n-1}}$  and  $\bar{\mathbf{q}}_{i+1,j_{d_{n-1}},k+d_{n-1}}$  both exist, until one does not. Then the previous  $d_{n-1}$  yields the  $L(n - 1, j, k)$ .

Assuming that for all  $j'$  and  $k'$ , we have computed  $L(i + 1, j', k')$ , we will use the computed  $L(i + 1, j', k')$  to recursively calculate  $L(i, j, k)$ . For any  $\bar{\mathbf{q}}_{i,j,k}$ , set  $d_i = 0$ . Traversing  $j'$  and check if  $\bar{\mathbf{q}}_{i+1,j',k}$  satisfies constraints on joint angles and velocities. If there are no joint angles that satisfy the constraints, it indicates that the manipulator is stuck at the current joint angles and cannot proceed to the next step. Otherwise, there exists a  $j_0$  such that  $\bar{\mathbf{q}}_{i+1,j_0,k}$  satisfies the constraints and has the maximum  $L(i + 1, j_0, k)$ . If  $L(i + 1, j_0, k) = 0$ , we have  $L(i, j, k) = 0$  and stop the increment on  $d_i$ .

Then we move on to  $d_i = 1$ . We traverse  $\bar{\mathbf{q}}_{i+1,j',k-1}$  and  $\bar{\mathbf{q}}_{i+1,j',k+1}$ , and check if constraints on joint angles and velocities are satisfied. If there exist  $j_{-1}, j_1$  such that  $\bar{\mathbf{q}}_{i+1,j_{-1},k-1}$  and  $\bar{\mathbf{q}}_{i+1,j_1,k+1}$  satisfy the constraints respectively, and  $L(i, j_{\pm 1}, k \pm 1) \geq d_i$ , by the recursive property, we have  $L(i, j, k) \geq d_i$ . Otherwise,  $L(i, j, k) = 0$ ;

Subsequently, we increase on  $d_i$  by 1 at each step, traverse  $\bar{\mathbf{q}}_{i+1,j',k-d_i}$  and  $\bar{\mathbf{q}}_{i+1,j',k+d_i}$ . If constraints cannot be satisfied, or any  $L(i + 1, j, k + t)$  for  $t \in \{-d_i, -d_i + 1, \dots, d_i\}$  is less than  $d_i$ , we have  $L(i, j, k) = d_i - 1$ , and stop the increment on  $d_i$ .

Through the aforementioned recursion, we can compute all the values of  $L(i, j, k)$ . Subsequently, from  $L(0, j, 0)$ , we select the maximum value  $L(0, j_0, 0)$ , which represents the maximum  $d$ . The corresponding  $\bar{\mathbf{q}}_{0,j_0,0}$  is then used as the inverse kinematic solution for the starting point of the path. Algorithm 1 shows the solution.

During the motion of the manipulator, the  $c_i$  corresponding to the  $i$ th sampling point is read in real-time. Suppose  $\bar{\mathbf{q}}_{i-1,j_{c_i-1}}$  is the joint angles at the  $(i - 1)$ -th sampling point, then  $\bar{\mathbf{q}}_{i,j',c_i} = f^{-1}(\hat{\mathbf{T}}_{EEi}(b_{c_i}), \bar{\mathbf{q}}_{i,j,k})$  is used as the  $i$ -th sampling point's joint angle. This value is then sent to the manipulator, enabling it to move along the adjusted path.

### 3.3. Motion Compensation

In our study, we have only considered constraints on joint angle and velocity. However, in practical manipulator

---

#### Algorithm 1 The solution for the maximum value of $d$

---

```

Set  $i = n - 1$ 
Set  $d_i = 0$ 
For  $1 \leq j \leq m, -o \leq k \leq o$ 
repeat
  If compliant solutions  $\bar{\mathbf{q}}_{i+1,j_{\pm d_i},k_{\pm d_i}}$  both exist
     $d_i = d_i + 1$ 
  Else,  $L(i, j, k) = d_i - 1$ 
until  $L(i, j, k)$  is found

For  $(n - 1 > i \geq 0)$ 
  For  $1 \leq j \leq m, -o \leq k \leq o$ 
repeat
  If compliant solutions  $\bar{\mathbf{q}}_{i+1,j_{\pm d_{i-1}},k_{\pm d_{i-1}}}$  both exist
    And  $L(i + 1, j_t, k + t) \geq \delta_i$  for  $t \in \{-d_i, -d_i + 1, \dots, d_i\}$ 
       $d_i = d_i + \theta$ 
    Else,  $L(i, j, k) = d_i - 1$ 
until  $L(i, j, k)$  is found

Find  $j_0$ , such that:
 $L(0, j_0, 0) = \max_{j=1}^m L(0, j, 0)$ 
Denote  $\bar{\mathbf{q}}_{0,j_0,0}$  as the starting point of the path
 $d_{max} = L(0, j_0, 0)$ 

```

---

operations, there are also limitations on joint acceleration and jerk. Therefore, when testing the algorithm on the actual manipulators, adjustments to the algorithmic results are necessary to conform to these additional constraints.

We have chosen to employ a motion compensation algorithm. Due to the time intervals between sampling points along the path being greater than the communication cycle of the manipulator, the host system needs to communicate with the manipulator and issue control commands between adjacent sampling points. The target joint angles at intermediate points need to be obtained through interpolation or similar methods. To ensure smooth motion, we aim for the manipulator's joints to move at a constant speed between adjacent sampled points.

During communication between the host system and the manipulator, real-time readings of the current joint angles  $\mathbf{q}_{now}$ , velocities  $\dot{\mathbf{q}}_{now}$ , and accelerations  $\ddot{\mathbf{q}}_{now}$  of joints are obtained. Adjustment coefficients read at the last sampling point and the algorithmically derived path are used to calculate the expected joint angles  $\mathbf{q}_{i+1}$  at the next sampling point. Subsequently, the remaining time before the next sampling point, denoted as  $t_r$ , is used to compute the expected velocity  $\dot{\mathbf{q}}_d$ , acceleration  $\ddot{\mathbf{q}}_d$  and jerk  $\dddot{\mathbf{q}}_d$  for the next communication cycle:

$$\begin{aligned}
\dot{\mathbf{q}}_d &= \frac{\mathbf{q}_{i+1} - \mathbf{q}_{\text{now}}}{t_f} \\
\ddot{\mathbf{q}}_d &= \frac{\dot{\mathbf{q}}_d - \dot{\mathbf{q}}_{\text{now}}}{t_0} \\
\dddot{\mathbf{q}}_d &= \frac{\ddot{\mathbf{q}}_d - \ddot{\mathbf{q}}_{\text{now}}}{t_0}
\end{aligned} \tag{14}$$

where  $t_0$  is the communication period of the manipulator.

Subsequently, we sequentially examine whether the jerk, acceleration, and velocity exceed their respective limits. If any of these values surpass the limits, they need to be adjusted to their corresponding maximum values. Subsequently, the other two motion parameters need to be recalculated until all motion parameters comply with the constraints.

Considering the constraint on jerk, the manipulator may not be able to change the acceleration direction in a short time. After accelerating, if the manipulator needs to decelerate in a certain joint, there will still be a period of acceleration. This acceleration period might cause the joint angle to exceed its velocity limits. Therefore, a "cautionary value" needs to be set for the joint velocities. When the velocity surpasses this limit, the manipulator must reduce its acceleration and begin deceleration.

We can simulate the extreme scenarios for each joint, considering the need for the manipulator to immediately cease acceleration and begin deceleration when operating at maximum acceleration. At this point, the jerk reaches its upper limit and is opposite in direction to the current velocity. Assuming the velocity at the current communication point is 0, we can calculate the velocities and accelerations for the subsequent communication points. The velocity when the acceleration is 0 represents the velocity we need to reserve for the deceleration process. Subtracting this reserved velocity from the maximum velocity yields the cautionary value for velocity.

Similarly, due to the constraint on manipulator acceleration, when the manipulator velocity needs to change direction, there will still be a short deceleration along the current direction. This deceleration may cause the joint angles to exceed their limits. Consequently, when using the algorithm to solve the inverse kinematics, the joint angle limits need to be reduced to accommodate space for deceleration.

Figure 5 succinctly illustrates our motion compensation algorithm. The interpolated expected path points cannot guarantee that acceleration and jerk constraints are satisfied, hence we can only modify the actual path under these constraints. This process inevitably leads to discrepancies between the actual and theoretical paths, and our algorithm minimizes this error to the greatest extent under joint constraints, ensuring that the manipulator smoothly reaches the expected joint angles at the next sampling point.

For more extreme scenarios, such as when a joint of the manipulator initially moves in the direction of increasing joint angles at maximum velocity and acceleration, and subsequently, according to the algorithm's result, needs to

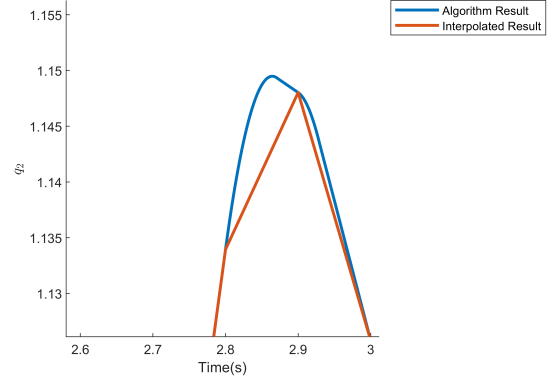


**Figure 5:** The interpolated expected path points cannot guarantee that acceleration and jerk constraints are satisfied, hence we can only modify the actual path under these constraints. This process inevitably leads to discrepancies between the actual and theoretical paths, and our algorithm minimizes this error to the greatest extent under joint constraints, ensuring that the manipulator smoothly reaches the expected joint angles at the next sampling point.

move in the opposite direction at maximum velocity, the error between the actual and expected joint angles will persist unchanged, since their maximum velocities are the same. Consequently, in order to minimize the duration of error existence and the magnitude of errors, we will impose further constraints on the joint angle velocities within the dynamic programming algorithm in section IIIB.

In addition, we also need to consider how to smoothly bring the manipulator to a stop as the motion approaches its end. This requires the manipulator's joint velocity, acceleration, and jerk to be zero as the motion stops. In order to smoothly bring the manipulator's velocity and acceleration to zero, additional constraints need to be satisfied:

$$\begin{aligned}
\ddot{\mathbf{q}} &\leq \ddot{\mathbf{q}}_{\text{max}} \cdot n_0 \cdot t_0 \\
\dot{\mathbf{q}} &\leq \dot{\mathbf{q}}_{\text{max}} \cdot n_0 \cdot t_0 - \frac{\ddot{\mathbf{q}}_{\text{max}}^2}{2 \cdot \ddot{\mathbf{q}}_{\text{max}}}
\end{aligned} \tag{15}$$

where  $n_0$  is the number of remaining communication cycles.

Thus, we have constructed the motion compensation algorithm for manipulator control. At each communication cycle, the final manipulator control algorithm is as described in Algorithm 2:

## 4. Results

To verify the feasibility of the proposed algorithm, we selected the Franka Emika manipulator for the research and testing of our algorithm. We will use the Cartesian path  $\mathbf{T}_{EE}(t)$  in equation (9) as the test path. In this path, the end effector of the manipulator will undergo an acceleration-deceleration motion tangential to a circular path with a radius of 0.1 meters, completing one full revolution.



---

**Algorithm 2** Motion Compensation
 

---

Read the elapsed time  $t$  of the motion

If  $t$  is the  $i$ -th sampling point

  Calculate  $c_{i+1}$

$$\mathbf{q}_{i+1} = f^{-1}(\hat{\mathbf{T}}_{EEi+1}(b_{c_{i+1}}), \mathbf{q}_i)$$

  Calculate the remaining time  $t_r$  before  $\hat{\mathbf{T}}_{EEi+1}(b_{c_{i+1}})$

$$\ddot{\mathbf{q}}_{\max}' = \max(\ddot{\mathbf{q}}_{\max}, \ddot{\mathbf{q}}_{\max} \cdot n_0 \cdot t_0)$$

$$\dot{\mathbf{q}}_{\max}' = \max(\dot{\mathbf{q}}_{\max}, \dot{\mathbf{q}}_{\max} \cdot n_0 \cdot t_0 - \frac{\ddot{\mathbf{q}}_{\max}^2}{2 \cdot \ddot{\mathbf{q}}_{\max}'})$$

  Read  $\mathbf{q}_{\text{now}}$ ,  $\dot{\mathbf{q}}_{\text{now}}$ , and  $\ddot{\mathbf{q}}_{\text{now}}$

$$\dot{\mathbf{q}}_d = \frac{\mathbf{q}_{i+1} - \mathbf{q}_{\text{now}}}{t_r}$$

$$\ddot{\mathbf{q}}_d = \frac{\dot{\mathbf{q}}_d - \dot{\mathbf{q}}_{\text{now}}}{t_0}$$

$$\ddot{\mathbf{q}}_d = \frac{\ddot{\mathbf{q}}_d - \ddot{\mathbf{q}}_{\text{now}}}{t_0}$$

\*For  $1 \leq c \leq 7$

  If  $\ddot{\mathbf{q}}_{dc} > \ddot{\mathbf{q}}_{\max c}$

$$\ddot{\mathbf{q}}_{dc} = \ddot{\mathbf{q}}_{\max c}, \ddot{\mathbf{q}}_{dc} = \ddot{\mathbf{q}}_{\text{now}c} + \ddot{\mathbf{q}}_{dc} \cdot t_0,$$

$$\dot{\mathbf{q}}_{dc} = \dot{\mathbf{q}}_{\text{now}c} + \ddot{\mathbf{q}}_{dc} \cdot t_0, \text{ return to } *$$

  If  $\dot{\mathbf{q}}_{dc} > \dot{\mathbf{q}}_{\max'c}$

$$\dot{\mathbf{q}}_{dc} = \dot{\mathbf{q}}_{\max'c}, \ddot{\mathbf{q}}_{dc} = \frac{\dot{\mathbf{q}}_{\text{now}c} - \dot{\mathbf{q}}_{dc}}{t_0},$$

$$\ddot{\mathbf{q}}_{dc} = \dot{\mathbf{q}}_{\text{now}c} + \ddot{\mathbf{q}}_{dc} \cdot t_0, \text{ return to } *$$

  If  $\mathbf{q}_{dc} > \mathbf{q}_{\max'c}$

$$\mathbf{q}_{dc} = \mathbf{q}_{\max'c}, \ddot{\mathbf{q}}_{dc} = \frac{\dot{\mathbf{q}}_{\text{now}c} - \dot{\mathbf{q}}_{dc}}{t_0},$$

$$\ddot{\mathbf{q}}_{dc} = \frac{\dot{\mathbf{q}}_{\text{now}c} - \dot{\mathbf{q}}_{dc}}{t_0}, \text{ return to } *$$

$$\mathbf{q}_d = \mathbf{q}_{\text{now}} + \dot{\mathbf{q}} \cdot t_0$$

  Return  $\mathbf{q}_d$  as the expected joint angle for the next communication point.

---

#### 4.1. Comparison with the Franka Cartesian pose generator

The manipulator has a Cartesian pose generator that can calculate the inverse kinematic solution of the Cartesian pose based on the current state of the manipulator and control its movements accordingly at a fixed frequency. The Cartesian pose generator is an online algorithm, which may lead to interruptions in subsequent motions. The Cartesian pose generator is used as a baseline algorithm in our comparative experiment. In this section, we will compare the Cartesian pose generator with the proposed algorithm on the original path.

First, we conducted tests on the proposed algorithm. For the original path, we simulated the joint angles of the manipulator at each communication point using software, obtaining the theoretical results of the algorithm. Additionally, we performed real-world testing using the Franka manipulator, resulting in laboratory results. Whether in simulation or in real-world testing, the manipulator completed the entire motion along the path, and the executed trajectory closely matched the expected path, as is shown in Figure 6.

Subsequently, we computed the angles, velocities, accelerations, and jerks of each joint in the simulated tests, as depicted in Figure 7. All the data has been normalized, with 1 representing its maximum value and -1 representing

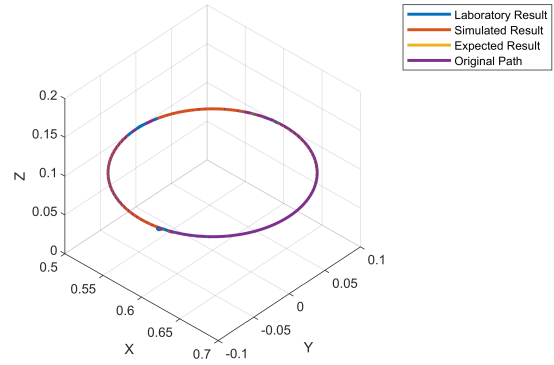


**Figure 6:** The end-effector paths obtained from both simulated and laboratory tests of the manipulator. Whether in simulation or in real-world testing, the manipulator completed the entire motion along the path, and the executed trajectory closely matched the expected path.

its minimum value. From the figures, it is evident that all motion parameters adhere to their respective constraints.

The testing of the Franka Cartesian pose generator, however, did not proceed as smoothly. To maintain control over variables, we initiated the manipulator from the same initial joint angles as the proposed algorithm. Due to joint velocities and accelerations exceeding limits, the manipulator was forced to halt shortly after commencing its motion. Consequently, we had to modify the path velocity to allow for a gradual acceleration of the manipulator. While the manipulator successfully initiated motion, it was compelled to stop due to joint angles surpassing their limits, just after the halfway point of the motion. The end-effector trajectory of the manipulator is illustrated in Figure 8.

Upon inspecting the motion parameters of each joint angle, we discovered that the angle of joint 7 reached its minimum value, resulting in an inability to continue the motion. The angle, velocity, acceleration, and jerk of joint 7 are illustrated in Figure 9, with each datum undergoing the same normalization process as depicted in Figure 7.

Subsequently, we compared the results obtained from the proposed algorithm with those from the Cartesian pose generator in Figure 10. It is visually apparent that while both methods initiated from the same initial joint angles, as the motion progressed, there were variations in the selection of joint angles. Under the proposed algorithm, the manipulator returns to its original pose, whereas under the Franka algorithm, the manipulator stops midway.

Through comparison, we can observe the drawbacks of the online planning algorithm. Without a holistic consideration of the entire path, there is a possibility of interruptions in subsequent motions. Offline planning cannot guarantee that the manipulator will move along the prescribed path without interruptions, let alone make adjustments. Conversely, the offline planning algorithm proposed in this paper, due to its advance consideration of all path points, can effectively ensure the completeness of the motion.

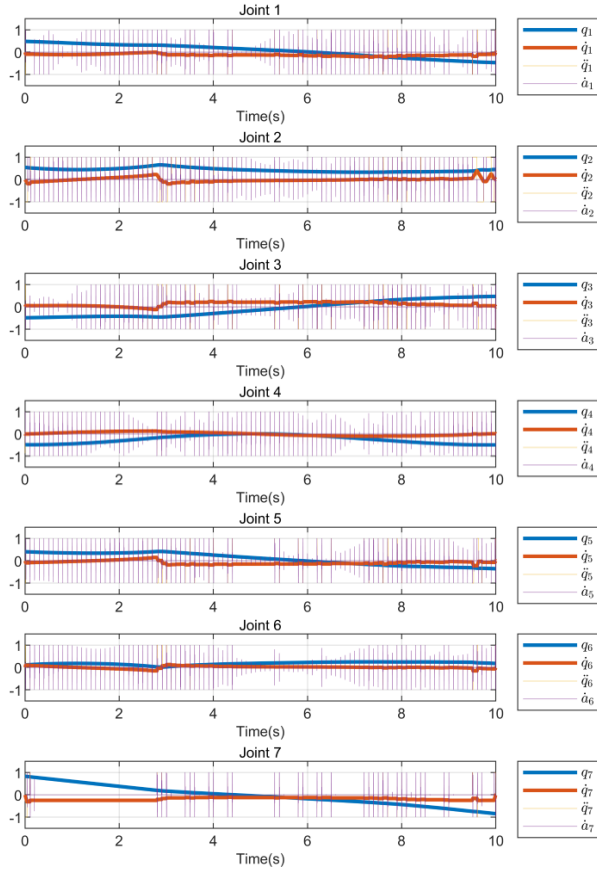


**Figure 7:** The angles, velocities, accelerations, and jerks of each joint in the simulated tests. All the data has been normalized, with 1 representing its maximum value and -1 representing its minimum value. From the figures, it is evident that all motion parameters adhere to their respective constraints.

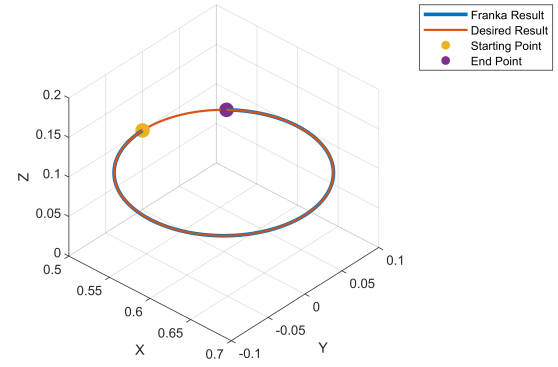
#### 4.2. Tests with real-time adjustments

Next, we tested the real-time adjustment capability of the proposed algorithm. We randomly generated a set of adjustment coefficients  $\{y_n\}$ , and as the manipulator operated, we sequentially input these coefficients, simulating the real-time data acquisition process. The randomly generated parameters, compared to real-world scenarios, can induce faster variations and better facilitate the comparison between algorithm results and the expected path.

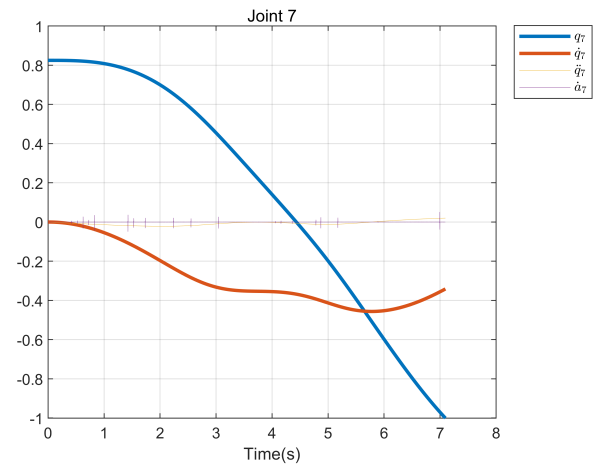
We conducted both simulated and real-world experiments simultaneously. Simulated experiments can eliminate errors and contingencies inherent to the manipulator itself, enabling a more effective evaluation of the algorithm's performance. Real-world experiments primarily serve to demonstrate the feasibility of the algorithm.

Figure 11 illustrates the real-world testing results incorporating real-time path adjustments. The manipulator completed the entire motion along the path seamlessly.

Then we compared the results of the simulated experiments, real-world experiments, and the expected path, as illustrated in Figure 12. It is evident that both in simulated and real-world testing, the manipulator completed the entire



**Figure 8:** The end-effector trajectory of the manipulator using Franka Cartesian pose generator. The manipulator compelled to stop due to joint angles surpassing their limits.



**Figure 9:** The angle, velocity, acceleration, and jerk of joint 7, with each datum undergoing the same normalization process as depicted in Figure 6. The angle of joint 7 reached its minimum value, resulting in an inability to continue the motion.

motion along the path, and the motion path closely aligned with the expected trajectory.

Subsequently, we computed the error in the algorithm results. To intuitively demonstrate the error, we only considered the positional error along the path. We calculated the Cartesian distance between the actual positions of the manipulator and their expected positions, as depicted in Figure 13.

The error exhibits periodic variation, with relatively smaller errors at the sampling points and larger errors at the interpolated waypoints. The magnitude of the maximum error is on the order of  $10^{-3}$  meters. This error can be mitigated using simple methods such as incorporating springs.

We further analyzed the sources of the error, which primarily stem from two aspects: Firstly, the algorithm employs interpolation to calculate joint angles for points outside the sampled path. Due to the non-linearity of the manipulator's

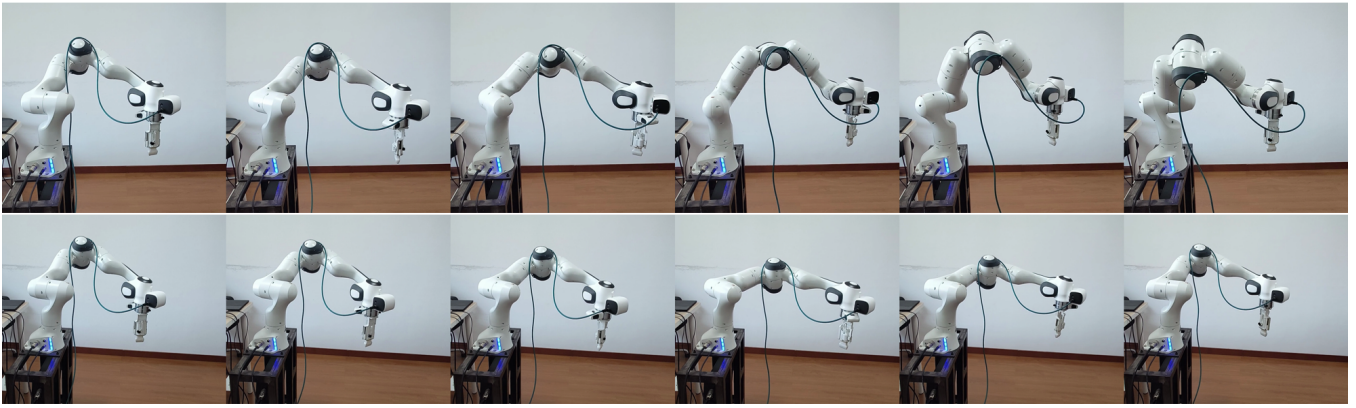


**Figure 10:** The top row illustrates the results obtained from the proposed algorithm, while the bottom row shows the results of the Franka algorithm. While both methods initiated from the same initial joint angles, as the motion progressed, there were variations in the selection of joint angles. Under the proposed algorithm, the manipulator returns to its original pose, whereas under the Franka algorithm, the manipulator stops midway.

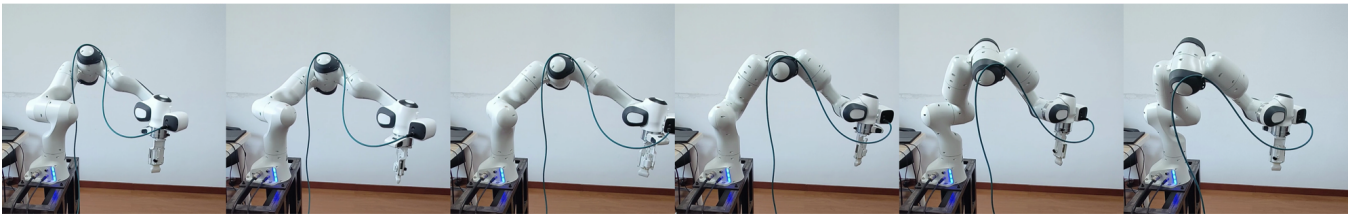


**Figure 11:** The real-world testing results incorporating real-time path adjustments. The manipulator completed the entire motion along the path seamlessly.

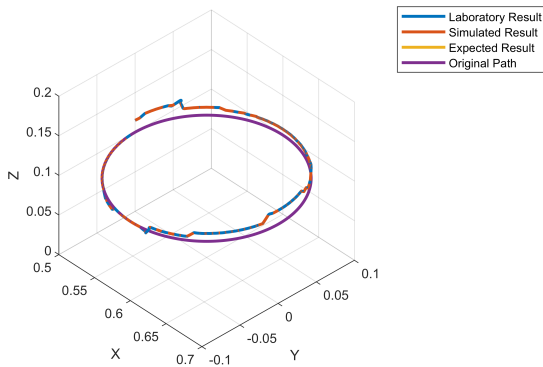


**Figure 12:** The end-effector paths obtained from both simulated and laboratory tests of the manipulator. Whether in simulation or in real-world testing, the manipulator completed the entire motion along the path, and the executed trajectory closely matched the expected path.

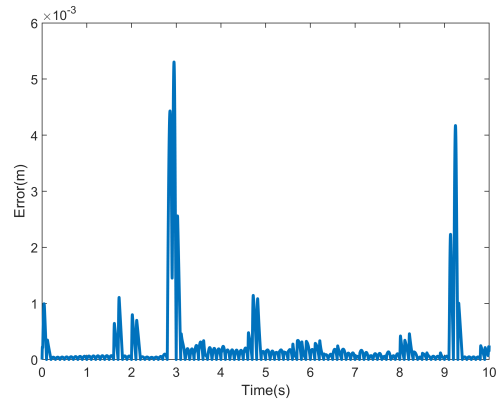
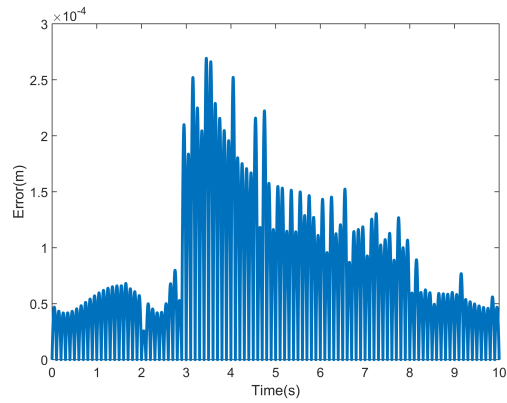


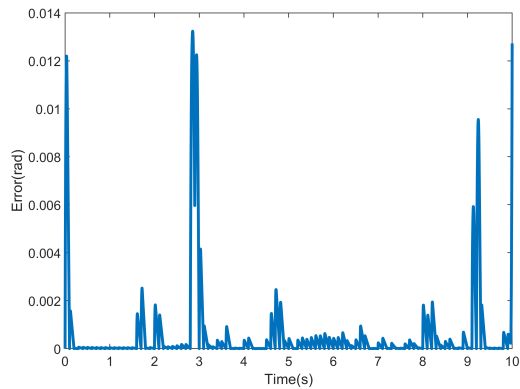
**Figure 13:** The Cartesian distance between the actual positions of the manipulator and their expected positions. The error exhibits periodic variation, with relatively smaller errors at the sampling points and larger errors at the interpolated waypoints. The magnitude of the maximum error is on the order of  $10^{-3}$  meters. This error can be mitigated using simple methods such as incorporating springs.

kinematic mapping, there exist discrepancies between the interpolated Cartesian poses and the expected poses. Secondly, the motion compensation algorithm, utilized to adhere to acceleration and jerk constraints, introduces additional error between the actual manipulator joint angles and the interpolated results. Consequently, we separately computed these two error components, as depicted in Figures 14.

The error between the interpolated results and the expected path is approximately an order of magnitude smaller than the error between the algorithm results and the expected path. The error between the joint angles obtained by the algorithm and those obtained by interpolation is relatively small at most path points. However, at certain individual



(a) Interpolated Path Error



(b) Motion Compensation Error

**Figure 14:** The error between the interpolated results and the expected path is plotted in (a), and the error generated by motion compensation is plotted in (b). By comparing these error components, it becomes evident that the primary source of error originates from motion compensation.

points, the error sharply increases. These peak points of error generally correspond to the peak points of error between the algorithm results and the expected results. At these points, the joint angles undergo significant changes in velocity, leading to an increase in motion compensation error.

By comparing these error components, it becomes evident that the primary source of error originates from motion compensation. For different manipulators with varying joint constraints, the motion compensation error also differs. Even considering the error introduced by motion compensation, the algorithm-calculated path closely aligns with the expected path, enabling the manipulator to effectively accomplish the designated tasks.

## 5. Conclusion

This paper proposes a dynamic programming-based offline redundancy resolution of redundant manipulators along prescribed paths with real-time adjustment. The manipulator will move along a path predefined by the user, while

simultaneously implementing adjustment on the manipulator's position along the normal to the path. Adjustment coefficients are obtained at a fixed frequency to achieve real-time position adjustment. The proposed algorithm utilizes dynamic programming to compute the maximum variation in adjustment coefficients. Given that the algorithm ensures real-time calculation of the manipulator's joint angles for the next sampling point, as long as the variation in adjustment parameters adheres to the defined constraints, the algorithm will guarantee the normal operation of the manipulator.

Through simulated and real-world experiments, the algorithm's computed joint path not only complies with the various constraints of the manipulator's joints, but also exhibits minimal deviation from the expected path, ensuring the precision and stability of the manipulator's operation.

The main innovation of this paper lies in augmenting traditional offline optimal planning with real-time adjustment capabilities, achieving a fusion of offline planning and online planning. Additionally, the utilization of dynamic programming enables the proposed algorithm to adjust the path of the manipulator to the maximum extent possible within the constraints of the hardware. The practical application value of this method extends to medical scanning and various similar scenarios.

## Acknowledgments

This work was supported by The National Natural Science Foundation(Nos.12090020, 12090025) and the Zhejiang Provincial Science and Technology Program(2022C03113).

## References

- Fahimi, F., 2009;2008;. *Autonomous Robots: Modeling, Path Planning, and Control*. 1. Aufl.;1; ed., Springer Science + Business Media, New York, NY.
- Ferrentino, E., Chiacchio, P., . *Redundancy Parametrization in Globally-Optimal Inverse Kinematics*. Springer International Publishing, Cham. *Advances in Robot Kinematics* 2018, pp. 47–55.
- Ferrentino, E., Savino, H.J., Franchi, A., Chiacchio, P., 2023. A dynamic programming framework for optimal planning of redundant robots along prescribed paths with kineto-dynamic constraints. *IEEE transactions on automation science and engineering* , 1–14.
- Ficuciello, F., Villani, L., Siciliano, B., 2015. Variable impedance control of redundant manipulators for intuitive human-robot physical interaction. *IEEE transactions on robotics* 31, 850–863.
- Haddadin, S., Parusel, S., Johannsmeier, L., Golz, S., Gabl, S., Walch, F., Sabaghian, M., Jaehne, C., Hausperger, L., Haddadin, S., 2022. The franka emika robot: A reference platform for robotics research and education. *IEEE robotics and automation magazine* 29, 2–20.
- He, W., Dong, Y., Sun, C., 2016. Adaptive neural impedance control of a robotic manipulator with input saturation. *IEEE transactions on systems, man, and cybernetics. Systems* 46, 334–344.
- He, Y., Liu, S., 2021. Analytical inverse kinematics for franka emika panda - a geometrical solver for 7-dof manipulators with unconventional design, *IEEE*. pp. 194–199.
- Hogan, N., 1984. Impedance control: An approach to manipulation, *IEEE*. pp. 304–313.
- Lee, S., Bejczy, A.K., 1991. Redundant arm kinematic control based on parameterization, *IEEE Comput. Soc. Press*. pp. 458–465 vol.1.
- Li, K., Xu, Y., Meng, M.Q., 2021. An overview of systems and techniques for autonomous robotic ultrasound acquisitions. *IEEE transactions on medical robotics and bionics* 3, 510–524.

- Ma, L.Z., Yao, G.Y., Ni, Q.L., Zhu, Z., 2005. Study of the traditional chinese medicine(tcm) massage robot based on the hybrid mechanism to obtain rolling treatment. *Jixie sheji yu yanjiu* 21, 43–46.
- Schappler, M., 2023. Pose optimization of task-redundant robots in second-order rest-to-rest motion with cascaded dynamic programming and nullspace projection, in: Gusikhin, O., Madani, K., Nijmeijer, H. (Eds.), *Informatics in Control, Automation and Robotics*, Springer International Publishing, Cham. pp. 106–131.
- Shimizu, M., Kakuya, H., Yoon, W., Kitagaki, K., Kosuge, K., 2008. Analytical inverse kinematic computation for 7-dof redundant manipulators with joint limits and its application to redundancy resolution. *IEEE transactions on robotics* 24, 1131–1142.
- Simpson, M.G., 1961. An introduction to dynamic programming. *Applied Statistics* 10, 32–38.
- Song, P., Yu, Y., Zhang, X., 2017. Impedance control of robots: An overview, *IEEE*. pp. 51–55.
- Tittel, S., 2021. Analytical solution for the inverse kinematics problem of the franka emika panda seven-dof light-weight robot arm, *IEEE*. pp. 1042–1047.
- Xenya, M.C., Cortesao, R., 2023. A compliant robot-assisted mold polishing application using the franka emika robot, *IEEE*. pp. 1–7.
- Xu, Q., Sun, X., 2018. Adaptive operation-space control of redundant manipulators with joint limits avoidance, *IEEE*. pp. 358–363.
- Zeng, X., Zhu, G., Gao, Z., Ji, R., Ansari, J., Lu, C., 2023. Surface polishing by industrial robots: a review. *International journal of advanced manufacturing technology* 125, 3981–4012.
- Zhang, Y., Li, S., Zhou, X., 2019. Recurrent-neural-network-based velocity-level redundancy resolution for manipulators subject to a joint acceleration limit. *IEEE transactions on industrial electronics* (1982) 66, 3573–3582.
- Zhong, L., Zhang, X., Zhai, X., Li, Y., Xu, Z., Pan, J., Zhou, X., 2023. Real-time solution of multi-constrained quadratic programming problem for redundant manipulator based on recurrent neural network, *IEEE*. pp. 1–6.
- Zietz, J., 2007. Dynamic programming: An introduction by example. *The Journal of economic education* 38, 165–186.